CAUCHY – Jurnal Matematika Murni dan Aplikasi
Volume 11 (2) (2026), Pages 2740–2764
p-ISSN: 2086-0382; e-ISSN: 2477-3344

Dynamic Analysis of a Tuberculosis Epidemic Model in Children Considering the Progression of Stunting Condition from Moderate to Severe

Ranti Rivani Aisyah*[1], Nursanti Anggriani[2], and Anita Triska[2]

[1] *Master's Program in Mathematics, Faculty of Mathematics and Natural Sciences, Universitas Padjadjaran, Sumedang, Indonesia*
[2] *Department of Mathematics, Faculty of Mathematics and Natural Sciences, Universitas Padjadjaran, Sumedang, Indonesia*

Abstract

Poor nutritional status, particularly stunting, increases susceptibility to tuberculosis (TB) infection, while TB can further worsen nutritional status and contribute to the progression of stunting, indicating a bidirectional relationship between TB and nutritional status. Among mathematical epidemiological studies on TB and stunting, none has simultaneously integrated a population of children, the progression of stunting from moderate to severe, and an environmental disease reservoir within a single model. Therefore, this study aims to develop a mathematical epidemiological model that integrates these three aspects, conduct dynamical and stability analyses, perform sensitivity analysis, and conduct numerical simulations to illustrate the dynamics. Two equilibrium points are obtained, namely the disease-free equilibrium (DFE) and the endemic equilibrium (EE), along with the basic reproduction number $\mathcal{R}_0$. The Jacobian matrix is used to establish the local stability of the DFE when $\mathcal{R}_0 < 1$, while the *Center Manifold Theorem* shows that the model undergoes a forward bifurcation at $\mathcal{R}_0 = 1$, indicating a threshold between the disease-free state and TB persistence, with the EE being locally asymptotically stable for $\mathcal{R}_0 > 1$ sufficiently close to 1. Global sensitivity analysis using the Latin Hypercube Sampling–Partial Rank Correlation Coefficient (LHS-PRCC) method identifies $(\mu_B - \pi_B)$, β, c, e, and ϕ as the most influential parameters on $\mathcal{R}_0$. Numerical simulations show that reducing e or increasing c and γ can decrease the infected population, suggesting that limiting TB exposure, improving ventilation, and promoting early diagnosis and effective treatment may help reduce TB transmission.

Keywords: Tuberculosis; Stunting; Mathematical Model; Dynamical Analysis; Sensitivity Analysis.

Copyright © 2026 by Authors, Published by CAUCHY Group. This is an open access article under the CC BY-SA License (https://creativecommons.org/licenses/by-sa/4.0)

1. Introduction

Tuberculosis (TB) is an infectious disease caused by *Mycobacterium tuberculosis* (Mtb) and is transmitted via inhalation of droplet nuclei generated by individuals with active TB [1]. Approximately 10.7 million people developed TB worldwide in 2024, and an estimated 1.23 million died from the disease [2]. Although studies have examined the spectrum of TB infection [3, 4], the classical approach generally classifies TB infection into latent TB and active TB

*Corresponding author. E-mail: ranti20004@mail.unpad.ac.id

Received: September 9, 2026 Revised: November 3, 2026 Accepted: November 15, 2026
DOI: https://doi.org/10.18860/cauchy.v11i2.46004

[4]. TB in children is often difficult to diagnose due to its paucibacillary nature and atypical clinical manifestations [5, 6]. Infection risk is influenced by factors such as cigarette smoke, indoor air pollution, and malnutrition [7]. Poor ventilation increases airborne droplet nuclei concentrations [1], while household contact with TB patients increases children's infection risk 6.2-fold [8]. Studies have reported that Mtb can remain viable in environments for months to years [9], with high concentrations detected in environments occupied by TB patients [10–12].

Stunting is a form of chronic undernutrition characterized by low height-for-age, affecting approximately 149 million children worldwide in 2022 [13]. The global prevalence among children under five was estimated at 22% in 2020 [14]. Based on the *Height-for-Age Z-score* (HAZ), stunting is classified as moderate ($-3 < \text{HAZ} \leq -2$ SD) or severe ($\text{HAZ} \leq -3$ SD) [15]. Longitudinal studies in India and Nairobi have documented progression from moderate to severe stunting [16, 17], with 23% of children experienced this progression in Nairobi [17]. Since nutritional deficiencies can begin early in life, the first 1,000 days are critical for physical and mental development [18]. Furthermore, stunting can hinder physical growth and brain development [14] and impair immune function, increase susceptibility to infections including TB [19]

Poor nutritional status can increase the risk of TB by two to three times due to impaired immune function [19–21] and may also increase the risk of mortality [22]. Conversely, TB infection can further worsen nutritional status through inflammatory responses, increased metabolic demands, decreased appetite, and impaired nutrient absorption, creating a bidirectional cycle between the two conditions [19, 23]. If this deterioration in nutritional status persists chronically, it may further aggravate existing stunting or hinder nutritional recovery in children [14, 17, 24].

Some mathematical models have incorporated nutritional factors, particularly focusing on stunting in children [25], while others have considered TB-related factors such as co-infections with malaria and HIV/AIDS [26], mask use [27], education [28], or an environmental TB reservoir [29]. Amelia et al. [30] also incorporated stunting into a TB model, but considered the general population rather than children, who are vulnerable to the combined effects of TB and stunting [19, 21, 23, 24]. Although existing studies have addressed nutritional factors and environmental reservoirs, the progression from moderate to severe stunting has not been incorporated into a model of TB in children. This gap is important because TB and poor nutritional status can adversely affect each other [19, 21, 24]. Therefore, a model incorporating stunting severity progression is needed to represent the interaction between TB and nutritional status in children.

To address this limitation, this study develops a mathematical model of TB in children that incorporates nutritional status, progression from moderate to severe stunting, and an environmental reservoir. This framework provides a more integrated representation by conducting a comprehensive dynamical analysis, sensitivity analysis, and numerical simulations to investigate the effects of these factors on TB transmission in children.

The remainder of this paper is organized as follows: (1) Introduction; (2) Methods; (3) Model Formulation; (4) Dynamical Analysis; (5) Numerical Simulations; (6) Sensitivity Analysis and Parameter Variation; and (7) Conclusion and Discussion.

2. Methods

This study uses a mathematical model of TB in children while accounting for progression from moderate to severe stunting. The research procedures are as follows: (1) formulating the model based on assumptions, a schematic diagram, and parameter values; (2) determining the disease-free equilibrium (DFE), endemic equilibrium (EE), and basic reproduction number using the *Next Generation Matrix* (NGM) method; (3) analyzing the local stability of the DFE using Jacobian eigenvalues and investigating bifurcation behavior and EE stability using the *Center Manifold Theorem*; (4) performing numerical simulations to illustrate population dynamics and validate the analytical results; and (5) conducting global sensitivity analysis using *Latin Hypercube Sampling–Partial Rank Correlation Coefficient* (LHS-PRCC) to identify influential parameters and assess how uncertainty in parameter values affects the system dynamics.

3. Model Formulation

This study employs an SEIR model to describe the dynamics of TB in children, with compartments representing susceptible (S), latent TB (E), active TB (I), and recovered (R). Nutritional status is also classified as normal (indexed by N), moderate stunting (indexed by M), or severe stunting (indexed by S). An environmental reservoir of viable Mtb (B) is also incorporated. Thus, the model consists of eleven compartments: S_N, E_N, I_N, R_N, S_M, E_M, I_M, R_M, I_S, R_S, and B.

The model considers children aged 0–60 months (0–5 years), during which nutritional status may still change [17, 31, 32]. Children enter the model at a birth rate of π, with proportions p and $1-p$ born with normal nutritional status and moderate stunting, respectively, based on a report that 13% of children experienced stunting at birth [33]. The birth rate π is estimated using the *Crude Birth Rate* (CBR) [34]. The estimated annual number of births in Indonesia is scaled to the model population based on the ratio of its initial size to the national population.

The population of children is assumed to be closed, with individuals leaving the population upon reaching 60 months of age or through natural mortality, at rates μ_a and μ_d, respectively. Assuming an average residence time of five years, the aging-out rate μ_a is calculated as the reciprocal of this duration. The natural mortality rate μ_d is estimated from the under-five mortality rate (U5MR) [34], assuming a constant mortality hazard over the five-year period and converting the reported rate into an annual rate based on the corresponding survival probability. To simplify the analytical analysis, these two rates are combined into a single exit rate, $\mu = \mu_a + \mu_d$.

Children with normal nutritional status may progress to moderate stunting at rate ω, while children with moderate stunting may recover at rate η. Both rates are assumed, with $\omega > \eta$, reflecting the assumption that nutritional deterioration occurs faster than recovery. For simplicity, nutritional transitions are restricted to children who have not been infected with TB. TB transmission is characterized by the force of infection, $\xi = \frac{eB}{c+B}$, where e and c are assumed due to limited empirical data. The force of infection is ξ for children with normal nutritional status and $\phi\xi$ for those with moderate stunting, where $\phi > 1$ reflecting their increased susceptibility to TB [20, 21, 24]. Latent TB infection is assumed to be non-transmissible.

Progression from latent to active TB occurs at rates α_N and $\tau\alpha_M$ in children with normal nutritional status and moderate stunting, respectively. These rates are estimated from the age-specific risks of progression from latent to active TB as reported by Arregui et al. [35]. The reported cumulative progression probabilities are converted into continuous transition rates and averaged across age groups to obtain estimates for children aged 0–5 years. Due to limited data stratified by nutritional status, equal baseline rates are assumed. The multiplier $\tau > 1$ accounts for the increased risk of TB progression in children with moderate stunting [20].

Severe stunting is assumed to develop in children with moderate stunting and active TB at rate δ. This transition represents the potential worsening of nutritional status due to TB, which may exacerbate nutritional deterioration [19–21]. This simplifying assumption does not imply that severe stunting develops exclusively in children with active TB, excluding other progression pathways is a limitation of the model. The value of δ is adopted from Oduro et al. [17], based on the estimated baseline transition intensity from moderate to severe stunting without covariates, and converted from months^{-1} to years^{-1}. For simplicity, children who recover from TB are assumed to remain in their respective nutritional status throughout the modeling period.

TB-related mortality occurs at rates d, $\varepsilon_M d$, and $\varepsilon_S d$ in children with normal nutritional status, moderate stunting, and severe stunting, respectively. The factors ε_M and ε_S are introduced as risk multipliers to account for increased mortality associated with poorer nutritional status [36, 37], with $\varepsilon_S > \varepsilon_M > 1$. TB recovery occurs at rates γ_N, $\sigma_M\gamma_M$, and $\sigma_S\gamma_S$ in the respective nutritional statuses, with the same baseline recovery rates assumed [38]. The factors σ_M and σ_S account for potentially lower recovery rates among children with poorer nutritional status [36], with $\sigma_S < \sigma_M < 1$. For simplicity, permanent immunity following TB recovery is assumed, and reinfection is excluded from the model. This assumption is adopted to simplify the model

structure and does not imply that recovered children are biologically immune to reinfection.

The compartment B represents viable Mtb in the environmental reservoir that may contribute to TB transmission. Children with active TB contribute to this reservoir through bacterial shedding at rate β. Given that children have a lower capacity to generate infectious aerosols than adults [39], their contribution is assumed to be relatively small. The reservoir dynamics are represented by the difference between the bacterial growth rate and the rate of loss of viability, following the approach of Codeço [40]. The net rate, $\mu_B - \pi_B$, is assumed due to limited empirical data on the dynamics of viable Mtb in the environmental reservoir and represents a modeling assumption rather than a direct empirical estimate. Furthermore, $\mu_B > \pi_B$ is imposed to ensure a positive net bacterial loss rate, preventing unbounded reservoir growth in the absence of bacterial input from infected individuals. The schematic diagram is presented in Fig. 1.

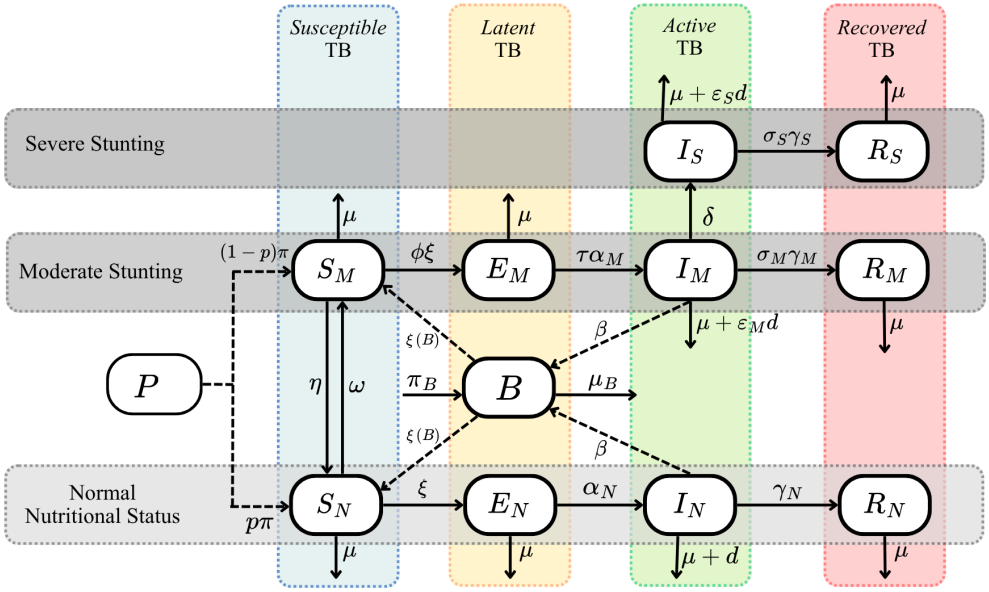


Fig. 1: Schematic diagram of the mathematical model of TB in children considering the progression of stunting from moderate to severe

Based on the schematic diagram in Fig. 1, the system is formulated as follows:

$$
\begin{aligned}
\frac{dS_N}{dt} &= p\pi + \eta S_M - (\omega + \xi + \mu)S_N, \\
\frac{dE_N}{dt} &= \xi S_N - (\alpha_N + \mu)E_N, \\
\frac{dI_N}{dt} &= \alpha_N E_N - (\gamma_N + \mu + d)I_N, \\
\frac{dR_N}{dt} &= \gamma_N I_N - \mu R_N, \\
\frac{dS_M}{dt} &= (1-p)\pi + \omega S_N - (\eta + \phi\xi + \mu)S_M, \\
\frac{dE_M}{dt} &= \phi\xi S_M - (\tau\alpha_M + \mu)E_M, \\
\frac{dI_M}{dt} &= \tau\alpha_M E_M - (\sigma_M\gamma_M + \delta + \mu + \varepsilon_M d)I_M, \\
\frac{dR_M}{dt} &= \sigma_M\gamma_M I_M - \mu R_M, \\
\frac{dI_S}{dt} &= \delta I_M - (\sigma_S\gamma_S + \mu + \varepsilon_S d)I_S,
\end{aligned}
\tag{1}
$$

$$\frac{dR_S}{dt} = \sigma_S \gamma_S I_S - \mu R_S,$$
$$\frac{dB}{dt} = \beta(I_N + I_M + I_S) - (\mu_B - \pi_B)B.$$

The force of infection $\xi = \frac{eB}{c+B}$ represents saturation in TB exposure from the environmental reservoir. The total exit rate from each compartment is defined as $\mu = \mu_d + \mu_a$. The variables and parameters, along with their descriptions, units, values, and sources, are presented in Table 1. Unless otherwise specified, all rates in Table 1 refer to the population of children. This is omitted from the parameter descriptions for brevity.

Table 1: Variables and parameters of the system (1)

Parameter	Description	Unit	Value	Source
π	Recruitment rate	child/year	1377	Calculated based on [34]
p	Proportion born without stunting	–	0.87	[33]
μ_d	Natural mortality rate	year^{-1}	0.0033	Calculated based on [34]
μ_a	Aging-out rate	year^{-1}	0.2	Calculated
$\mu_B - \pi_B$	Net loss rate of viable Mtb in the environmental reservoir	year^{-1}	0.121	Assumed
ω	Progression rate to moderate stunting	year^{-1}	0.2	Assumed
η	Progression rate to normal nutrition	year^{-1}	0.1	Assumed
δ	Progression rate to severe stunting	year^{-1}	1.7628	[17]
ϕ	Force-of-infection multiplier for moderate stunting	–	2.36	[21]
τ	TB activation rate multiplier for moderate stunting	–	1.96	[20]
α_N, α_M	TB activation rates in normal nutrition and moderate stunting	year^{-1}	0.318	Calculated based on [35]
γ_N, γ_M, γ_S	TB recovery rates in normal nutrition, moderate stunting, and severe stunting	year^{-1}	0.231	[38]
σ_M	TB recovery multiplier for moderate stunting	–	0.8	Assumed
σ_S	TB recovery multiplier for severe stunting	–	0.6	Assumed
d	TB-induced mortality rate	year^{-1}	0.389	[38]
ε_M	TB mortality rate multiplier in moderate stunting	–	2.22	[36]
ε_S	TB mortality rate multiplier in severe stunting	–	2.92	[36]
β	Rate of bacterial contribution to reservoir with active TB	cell/(child × year)	0.1	Assumed
c	Half-saturation constant of Mtb concentration in the environmental reservoir	cell	2500	Assumed
e	Contribution rate of active TB individuals to the environmental Mtb concentration	year^{-1}	0.7	Assumed

Since System (1) represents both the population of children and the environmental bacterial population, it is necessary to show that all solution variables remain nonnegative.

Lemma 1. *Let* $\mathbf{x}(0) \geq \mathbf{0}$*, where*

$$\mathbf{x}(t) = (x_1(t), x_2(t), \ldots, x_{11}(t))^T. \tag{2}$$

Then, the solutions $\mathbf{x}(t)$ *remain nonnegative for all* $t \geq 0$.

Proof. Consider the last equation of System (1). Since $\beta(I_N(t) + I_M(t) + I_S(t)) \geq 0$, it follows that:

$$\frac{dB(t)}{dt} \geq -(\mu_B - \pi_B)B(t).$$

With the assumption $\mu_B > \pi_B$, by integrating and substituting initial condition, we obtain:

$$B(t) \geq B(0)\exp[-(\mu_B - \pi_B)t] \geq 0. \tag{3}$$

Thus, $B(t) \geq 0$ for $t \geq 0$. Since $e > 0$, $c > 0$, and $B(t) \geq 0$, it follows that $\xi = \frac{eB}{c+B} \geq 0$. Using the same approach, it can be shown that:

$$\begin{aligned}
S_N(t) &\geq S_N(0)\exp\left[-\int_0^t (\omega + \xi + \mu)\,dt\right] \geq 0,\\
E_N(t) &\geq E_N(0)\exp[-(\alpha_N + \mu)t] \geq 0,\\
I_N(t) &\geq I_N(0)\exp[-(\gamma_N + \mu + d)t] \geq 0,\\
R_N(t) &\geq R_N(0)\exp[-\mu t] \geq 0,\\
S_M(t) &\geq S_M(0)\exp\left[-\int_0^t (\eta + \phi\xi + \mu)\,dt\right] \geq 0,\\
E_M(t) &\geq E_M(0)\exp[-(\tau\alpha_M + \mu)t] \geq 0,\\
I_M(t) &\geq I_M(0)\exp[-(\sigma_M\gamma_M + \delta + \mu + \varepsilon_M d)t] \geq 0,\\
R_M(t) &\geq R_M(0)\exp[-\mu t] \geq 0,\\
I_S(t) &\geq I_S(0)\exp[-(\sigma_S\gamma_S + \mu + \varepsilon_S d)t] \geq 0,\\
R_S(t) &\geq R_S(0)\exp[-\mu t] \geq 0.
\end{aligned} \tag{4}$$

Since all initial conditions are nonnegative, all terms on the right-hand sides of Eq. (3)–Eq. (4) are nonnegative. Therefore, all solutions of System (1) remain nonnegative for every $t \geq 0$. This ensures that all state variables remain biologically meaningful. □

Next, we establish a positively invariant region to ensure that the model solutions remain biologically meaningful and bounded for all $t \geq 0$. Let $N_C(t)$ denote the total population of children, given by $N_C(t) = S_N + E_N + I_N + R_N + S_M + E_M + I_M + R_M + I_S + R_S$, with $\mathbf{x}_C(t)$ denote the corresponding vector of children population compartments. The feasible regions for the population of children and the environmental Mtb reservoir are denoted by Λ_C and Λ_B, respectively.

Lemma 2. *The feasible region of System (1) is defined as* $\Lambda = \Lambda_C \times \Lambda_B \subset \mathbb{R}_+^{11}$, *where* $\Lambda_C = \{\mathbf{x}_C \in \mathbb{R}_+^{10} : N_C(t) \leq N_C^{\max}\}$ *and* $\Lambda_B = \{B \in \mathbb{R}_+ : B(t) \leq B^{\max}\}$. *This region is positively invariant, where* $N_C^{\max} = \max\left\{N_C(0), \frac{\pi}{\mu}\right\}$ *and* $B^{\max} = \max\left\{B(0), \frac{\beta N_C^{\max}}{\mu_B - \pi_B}\right\}$, *under the assumption* $\mu_B > \pi_B$.

Proof. By summing all equations governing the population of children in System (1) yields:

$$\frac{dN_C(t)}{dt} = \pi - \mu N_C - d\left(I_N + \varepsilon_M I_M + \varepsilon_S I_S\right).$$

Since all compartments and parameters are nonnegative, it follows that

$d\left(I_N + \varepsilon_M I_M + \varepsilon_S I_S\right) \geq 0$. Therefore:

$$\frac{dN_C(t)}{dt} + \mu N_C \leq \pi.$$

Using an integrating factor, we obtain:

$$N_C(t) \leq \frac{\pi}{\mu} + \left(N_C(0) - \frac{\pi}{\mu}\right) e^{-\mu t}.$$

Thus, for $t \geq 0$, the total population of children satisfies the following bounds:

$$N_C(t) \leq \max\left\{N_C(0), \frac{\pi}{\mu}\right\} =: N_C^{\max}, \qquad \limsup_{t\to\infty} N_C(t) \leq \frac{\pi}{\mu}. \tag{5}$$

Next, the viable Mtb in the environmental reservoir equation in System (1) equivalent to:

$$\frac{dB(t)}{dt} + (\mu_B - \pi_B)B = \beta(I_N + I_M + I_S).$$

Since $I_N + I_M + I_S \leq N_C^{\max}$ along from Eq. (5), it follows that:

$$\frac{dB(t)}{dt} + (\mu_B - \pi_B)B \leq \beta N_C^{\max}.$$

Under the assumption $\mu_B > \pi_B$, applying an integrating factor gives:

$$B(t) \leq \frac{\beta N_C^{\max}}{\mu_B - \pi_B} + \left(B(0) - \frac{\beta N_C^{\max}}{\mu_B - \pi_B}\right) e^{-(\mu_B - \pi_B)t}.$$

Thus, for $t \geq 0$, the viable Mtb in the environmental reservoir satisfies the following bounds:

$$B(t) \leq \max\left\{B(0), \frac{\beta N_C^{\max}}{\mu_B - \pi_B}\right\} =: B^{\max}, \qquad \limsup_{t\to\infty} B(t) \leq \frac{\beta N_C^{\max}}{\mu_B - \pi_B}. \tag{6}$$

On the boundaries $N_C = N_C^{\max}$ and $B = B^{\max}$, the corresponding derivatives satisfy:

$$\frac{dN_C}{dt} \leq \pi - \mu N_C^{\max} \leq 0, \qquad \frac{dB}{dt} \leq \beta N_C^{\max} - (\mu_B - \pi_B)B^{\max} \leq 0.$$

Hence, the solutions remain bounded and nonnegative for all $t \geq 0$. Therefore, $\Lambda = \Lambda_C \times \Lambda_B$ is a positively invariant region of System (1). □

4. Dynamical Analysis

The System (1) has two equilibrium points, namely the DFE and EE. The DFE represents the condition in which TB does not spread within the population and is obtained explicitly. The EE represents the condition in which TB persists within the population, is obtained implicitly, and depends on ξ^*. The basic reproduction number $\mathcal{R}_0$ is derived using the NGM approach. The local stability of the DFE is analyzed using Jacobian eigenvalues along with the theory of Metzler matrices, while the bifurcation behavior and local stability of the EE near $\mathcal{R}_0 = 1$ are investigated using the *Center Manifold Theorem*.

4.1. Disease-free equilibrium

The DFE is obtained by setting all derivatives in System (1) to zero. Thus, the DFE point, denoted by X^0, is given by:

$$
\begin{aligned}
X^0 &= \left\{S_N^0, E_N^0, I_N^0, R_N^0, S_M^0, E_M^0, I_M^0, R_M^0, I_S^0, R_S^0, B^0\right\} \\
&= \left\{\frac{\pi(\mu p+\eta)}{\mu(\eta+\mu+\omega)}, 0, 0, 0, \frac{\pi\left(\mu(1-p)+\omega\right)}{\mu(\eta+\mu+\omega)}, 0, 0, 0, 0, 0, 0\right\}.
\end{aligned} \tag{7}
$$

The DFE point X^0 indicates that in the absence of TB infection, all infected compartments and the environmental TB reservoir are zero, while the population is distributed only among the susceptible compartments. Since all parameters are assumed to be positive and $0 \leq p \leq 1$, all components of X^0 are nonnegative. Therefore, X^0 exists and belongs to the feasible region Λ.

4.2. Basic reproduction number

The basic reproduction number, $\mathcal{R}_0$, is derived using the NGM approach of van den Driessche and Watmough [41]. Following this approach, the infected subsystem, which comprises E_N, I_N, E_M, I_M, I_S, and B, as defined in System (1), is decomposed into the vector of new infection rates $\mathcal{F}$ and the vector of net transition rates between infected compartments $\mathcal{V}$. These vectors can then be expressed as:

$$
\mathcal{F} = \begin{bmatrix} f_{E_N} \\ f_{I_N} \\ f_{E_M} \\ f_{I_M} \\ f_{I_S} \\ f_B \end{bmatrix} = \begin{bmatrix} \dfrac{eB}{c+B} S_N^0 \\ 0 \\ \dfrac{\phi eB}{c+B} S_M^0 \\ 0 \\ 0 \\ 0 \end{bmatrix}, \tag{8}
$$

$$
\mathcal{V} = \begin{bmatrix} v_{E_N} \\ v_{I_N} \\ v_{E_M} \\ v_{I_M} \\ v_{I_S} \\ v_B \end{bmatrix} = \begin{bmatrix} (\alpha_N+\mu)E_N \\ -\alpha_N E_N + (\gamma_N+\mu+d)I_N \\ (\tau\alpha_M+\mu)E_M \\ -\tau\alpha_M E_M + (\sigma_M\gamma_M+\delta+\mu+\varepsilon_M d)I_M \\ -\delta I_M + (\sigma_S\gamma_S+\mu+\varepsilon_S d)I_S \\ -\beta(I_N+I_M+I_S) + (\mu_B-\pi_B)B \end{bmatrix}. \tag{9}
$$

The Jacobian matrices F and V are obtained by evaluating the partial derivatives of $\mathcal{F}$ and $\mathcal{V}$ from Eq. (8) and Eq. (9), with respect to the infected-state variables $\mathbf{x} = (E_N, I_N, E_M, I_M, I_S, B)^T$ at the DFE X^0. Substituting X^0 from Eq. (7) gives:

$$
F = \left[\frac{\partial f_i}{\partial x_j}\right]_{X^0} = \begin{bmatrix} 0 & 0 & 0 & 0 & 0 & \dfrac{e\pi(\mu p+\eta)}{c\mu(\eta+\mu+\omega)} \\ 0 & 0 & 0 & 0 & 0 & 0 \\ 0 & 0 & 0 & 0 & 0 & \dfrac{e\pi\phi(\mu(1-p)+\omega)}{c\mu(\eta+\mu+\omega)} \\ 0 & 0 & 0 & 0 & 0 & 0 \\ 0 & 0 & 0 & 0 & 0 & 0 \\ 0 & 0 & 0 & 0 & 0 & 0 \end{bmatrix}. \tag{10}
$$

$$
V = \left[\frac{\partial v_i}{\partial x_j}\right]_{X^0} = \begin{bmatrix} b_1 & 0 & 0 & 0 & 0 & 0 \\ -\alpha_N & b_2 & 0 & 0 & 0 & 0 \\ 0 & 0 & b_3 & 0 & 0 & 0 \\ 0 & 0 & -\tau\alpha_M & b_4 & 0 & 0 \\ 0 & 0 & 0 & -\delta & b_5 & 0 \\ 0 & -\beta & 0 & -\beta & -\beta & \mu_B-\pi_B \end{bmatrix}. \tag{11}
$$

where $b_1 = \alpha_N + \mu$, $b_2 = \gamma_N + \mu + d$, $b_3 = \tau\alpha_M + \mu$, $b_4 = \sigma_M\gamma_M + \delta + \mu + \varepsilon_M d$, and $b_5 = \sigma_S\gamma_S + \mu + \varepsilon_S d$. The basic reproduction number is defined as $\mathcal{R}_0 = \rho(FV^{-1})$, where ρ denotes the spectral radius. Evaluating F and V at X^0 yields:

$$\mathcal{R}_0 = \frac{\beta e\pi\left[\alpha_N b_3 b_4 b_5(\mu p + \eta) + \tau\alpha_M b_1 b_2 \phi(\sigma_S\gamma_S + \delta + \mu + \varepsilon_S d)(\mu(1-p) + \omega)\right]}{c\mu(\eta + \mu + \omega)b_1 b_2 b_3 b_4 b_5(\mu_B - \pi_B)}, \tag{12}$$

Equation (12) expresses the basic reproduction number as the sum of two contributions, namely those from children with normal nutritional status and those with moderate stunting. Thus, it can be written as $\mathcal{R}_0 = \mathcal{R}_{0N} + \mathcal{R}_{0M}$, where:

$$\begin{aligned}
\mathcal{R}_{0N} &= \frac{\alpha_N \beta e\pi(\mu p + \eta)}{c\mu(\eta + \mu + \omega)(\alpha_N + \mu)(\gamma_N + \mu + d)(\mu_B - \pi_B)}, \\
\mathcal{R}_{0M} &= \frac{\tau\alpha_M \beta e\pi\phi(\sigma_S\gamma_S + \delta + \mu + \varepsilon_S d)(\mu(1-p) + \omega)}{c\mu(\eta + \mu + \omega)(\tau\alpha_M + \mu)(\sigma_M\gamma_M + \delta + \mu + \varepsilon_M d)(\sigma_S\gamma_S + \mu + \varepsilon_S d)(\mu_B - \pi_B)}.
\end{aligned} \tag{13}$$

Since all parameters are positive and $0 \le p \le 1$, it follows that $\mathcal{R}_0 \ge 0$. The basic reproduction number serves as a threshold for determining the potential for TB to persist in the population. Specifically, TB transmission tends to die out when $\mathcal{R}_0 < 1$, whereas TB may persist when $\mathcal{R}_0 > 1$.

4.3. Local stability analysis of disease-free equilibrium

The local stability of the DFE is analyzed by examining the eigenvalues of the Jacobian matrix evaluated at the DFE. Owing to the structure of the Jacobian matrix from System (1), five eigenvalues are determined directly. The stability of the remaining eigenvalues is then investigated using the theory of Metzler matrices, following the approach by Kamgang and Sallet [42].

Theorem 1. *The DFE, denoted by X^0, is locally asymptotically stable in the feasible region Λ if $\mathcal{R}_0 < 1$, and unstable if $\mathcal{R}_0 > 1$.*

Proof. Evaluating the Jacobian matrix of System (1) at the DFE yields five eigenvalues directly, namely:

$$\lambda_{1,2,3,4} = -\mu, \qquad \lambda_5 = -(\eta + \mu + \omega). \tag{14}$$

Since μ, η, and ω are positive, these five eigenvalues are strictly negative. The remaining part of the Jacobian is associated with the compartments E_N, I_N, E_M, I_M, I_S, and B. The corresponding reduced Jacobian is

$$J_r = \begin{pmatrix}
-b_1 & 0 & 0 & 0 & 0 & \frac{e}{c}S_N^0 \\
\alpha_N & -b_2 & 0 & 0 & 0 & 0 \\
0 & 0 & -b_3 & 0 & 0 & \frac{\phi e}{c}S_M^0 \\
0 & 0 & \tau\alpha_M & -b_4 & 0 & 0 \\
0 & 0 & 0 & \delta & -b_5 & 0 \\
0 & \beta & 0 & \beta & \beta & -b_6
\end{pmatrix}, \tag{15}$$

where $b_1, \ldots, b_5$ are defined as in Eq. (11) and $b_6 = \mu_B - \pi_B$. Since all off-diagonal entries of J_r are nonnegative, J_r is a Metzler matrix. According to Proposition 3.1 in Kamgang and Sallet [42], the matrix J_r can be partitioned as:

$$J_r = \begin{pmatrix} A & B \\ C & D \end{pmatrix}, \tag{16}$$

where A is a 5×5 matrix, B is a 5×1 matrix, C is a 1×5 matrix, and D is a scalar. The Metzler matrix J_r is stable if and only if both A and its Schur complement $D - CA^{-1}B$ are stable. Since A is lower triangular, its eigenvalues are $\lambda_{6,7,8,9,10} = -b_1, -b_2, -b_3, -b_4, -b_5$. Given that $b_i > 0$ for $i = 1, \ldots, 5$, A is a stable Metzler matrix. Hence, it remains to establish the Schur complement, $D - CA^{-1}B < 0$. A direct calculation using the definition of $\mathcal{R}_0$ from Eq. (12) yields:

$$D - CA^{-1}B = b_6(\mathcal{R}_0 - 1).$$

With the assumption $\mu_B > \pi_B$, yield $b_6 > 0$, and it follows that:

$$D - CA^{-1}B < 0 \quad \Longleftrightarrow \quad \mathcal{R}_0 < 1. \tag{17}$$

From Eq. (17) we can conclude that J_r is stable if and only if $\mathcal{R}_0 < 1$. Since the other five eigenvalues of J are negative, as shown in Eq. (14), and the reduced Jacobian matrix J_r is stable when $\mathcal{R}_0 < 1$, all eigenvalues of the Jacobian matrix evaluated at the DFE have negative real parts. Hence, the DFE is locally asymptotically stable in the feasible region Λ if $\mathcal{R}_0 < 1$. Conversely, if $\mathcal{R}_0 > 1$, then $D - CA^{-1}B > 0$, implying that J_r and, consequently, the DFE are unstable. Thus, $\mathcal{R}_0 = 1$ represents the threshold between the local stability of the DFE for $\mathcal{R}_0 < 1$ and its instability for $\mathcal{R}_0 > 1$. □

4.4. Endemic equilibrium

The EE represents a state of persistent TB infection and is obtained by setting all derivatives in System (1) to zero, with $I_N^*, I_M^*, I_S^*, B^* > 0$. The EE, denoted by X^*, is given by:

$$X^* = \{S_N^*, E_N^*, I_N^*, R_N^*, S_M^*, E_M^*, I_M^*, R_M^*, I_S^*, R_S^*, B^*\}, \tag{18}$$

with

$$S_N^* = \frac{\pi\left((\xi^*\phi + \mu)p + \eta\right)}{(\omega + \xi^* + \mu)(\xi^*\phi + \mu) + (\xi^* + \mu)\eta},$$

$$E_N^* = \frac{\xi^*\pi\left((\xi^*\phi + \mu)p + \eta\right)}{\left((\omega + \xi^* + \mu)(\xi^*\phi + \mu) + (\xi^* + \mu)\eta\right)(\alpha_N + \mu)},$$

$$I_N^* = \frac{\alpha_N\xi^*\pi\left((\xi^*\phi + \mu)p + \eta\right)}{\left((\omega + \xi^* + \mu)(\xi^*\phi + \mu) + (\xi^* + \mu)\eta\right)(\alpha_N + \mu)(\gamma_N + \mu + d)},$$

$$R_N^* = \frac{\gamma_N\alpha_N\xi^*\pi\left((\xi^*\phi + \mu)p + \eta\right)}{\left((\omega + \xi^* + \mu)(\xi^*\phi + \mu) + (\xi^* + \mu)\eta\right)(\alpha_N + \mu)(\gamma_N + \mu + d)\mu},$$

$$S_M^* = \frac{\pi\left((\xi^* + \mu)(1 - p) + \omega\right)}{(\omega + \xi^* + \mu)(\xi^*\phi + \mu) + (\xi^* + \mu)\eta},$$

$$E_M^* = \frac{\phi\xi^*\pi\left((\xi^* + \mu)(1 - p) + \omega\right)}{\left((\omega + \xi^* + \mu)(\xi^*\phi + \mu) + (\xi^* + \mu)\eta\right)(\tau\alpha_M + \mu)},$$

$$I_M^* = \frac{\tau\alpha_M\phi\xi^*\pi\left((\xi^* + \mu)(1 - p) + \omega\right)}{\left((\omega + \xi^* + \mu)(\xi^*\phi + \mu) + (\xi^* + \mu)\eta\right)(\tau\alpha_M + \mu)(\sigma_M\gamma_M + \delta + \mu + \varepsilon_M d)},$$

$$R_M^* = \frac{\sigma_M\gamma_M\tau\alpha_M\phi\xi^*\pi\left((\xi^* + \mu)(1 - p) + \omega\right)}{\left((\omega + \xi^* + \mu)(\xi^*\phi + \mu) + (\xi^* + \mu)\eta\right)(\tau\alpha_M + \mu)(\sigma_M\gamma_M + \delta + \mu + \varepsilon_M d)\mu},$$

$$I_S^* = \frac{\delta\tau\alpha_M\phi\xi^*\pi\left((\xi^* + \mu)(1 - p) + \omega\right)}{\left((\omega + \xi^* + \mu)(\xi^*\phi + \mu) + (\xi^* + \mu)\eta\right)(\tau\alpha_M + \mu)} \times (\sigma_M\gamma_M + \delta + \mu + \varepsilon_M d)(\sigma_S\gamma_S + \mu + \varepsilon_S d)$$

$$R_S^* = \frac{\sigma_S\gamma_S\delta\tau\alpha_M\phi\xi^*\pi\left((\xi^*+\mu)(1-p)+\omega\right)}{\left((\omega+\xi^*+\mu)(\xi^*\phi+\mu)+(\xi^*+\mu)\eta\right)(\tau\alpha_M+\mu)} \times (\sigma_M\gamma_M+\delta+\mu+\varepsilon_M d)(\sigma_S\gamma_S+\mu+\varepsilon_S d)\mu}$$

$$B^* = \frac{\xi^* c\mu(\eta+\mu+\omega)}{e\left((\omega+\xi^*+\mu)(\xi^*\phi+\mu)+(\xi^*+\mu)\eta\right)} \times \left[\mathcal{R}_0 + \xi^*\left(\mathcal{R}_{0N}\frac{p\phi}{\mu p+\eta} + \mathcal{R}_{0M}\frac{1-p}{\mu(1-p)+\omega}\right)\right]$$

The EE point is determined implicitly since B^* depends on ξ^*, while ξ^* is determined by B^* through the following relationship $\xi^* = \frac{eB^*}{c+B^*}$.

4.5. Existence analysis of the endemic equilibrium

In Eq. (18), since B^* appears implicitly in the components of the EE, its value is determined by substituting X^* into the definition of the force of infection, ξ^*, yielding the following polynomial equation:

$$\xi^*\left(s_2\xi^{*2} + s_1\xi^* + s_0\right) = 0, \tag{19}$$

where

$$\begin{aligned} s_2 = & -\left[\mu(1-p)(\mu p+\eta)(\eta+\mu+\omega)\mathcal{R}_{0M} + \mu p\phi(\mu(1-p)+\omega)(\eta+\mu+\omega)\mathcal{R}_{0N}\right. \\ & \left. + e\phi(\mu p+\eta)(\mu(1-p)+\omega)\right], \end{aligned}$$

$$\begin{aligned} s_1 = & -\mu(\mu p+\eta)(\mu(1-p)+\omega)(\eta+\mu+\omega)\mathcal{R}_0 + \mu e(1-p)(\mu p+\eta)(\eta+\mu+\omega)\mathcal{R}_{0M} \\ & + e\mu p\phi(\mu(1-p)+\omega)(\eta+\mu+\omega)\mathcal{R}_{0N} - e(\mu p+\eta)(\mu(1-p)+\omega)\left[\phi(\mu+\omega)+\eta+\mu\right], \end{aligned}$$

$$s_0 = e\mu(\mu p+\eta)(\mu(1-p)+\omega)(\eta+\mu+\omega)(\mathcal{R}_0-1).$$

Since ξ^* represents the force of infection, the root $\xi^* = 0$ from Eq. (19) corresponds to the DFE. Hence, only roots satisfying $\xi^* > 0$ are considered for the existence of biologically meaningful EE points. The corresponding positive roots are obtained from:

$$s_2\xi^{*2} + s_1\xi^* + s_0 = 0. \tag{20}$$

From Eq. (19), the sign of s_0 depends on $\mathcal{R}_0$. Moreover, $s_2 < 0$. Thus, the number of biologically meaningful EE points can be determined by analyzing the positive roots of Eq. (20) based on $\mathcal{R}_0$ and the sign of s_1.

Theorem 2. *The existence and number of biologically meaningful EE points of System (1) are determined by the positive real roots of Eq. (20). Specifically:*

(i) If $\mathcal{R}_0 < 1$ and $s_1 > 0$, System (1) may have one, two, or no biologically meaningful EE points according to the sign of D, where $D = s_1^2 - 4s_2s_0$. The existence of biologically meaningful EE points indicates the possibility of a backward bifurcation.

(ii) If $\mathcal{R}_0 < 1$ and $s_1 < 0$, System (1) has no biologically meaningful EE point.

(iii) If $\mathcal{R}_0 = 1$ and $s_1 > 0$, System (1) has one biologically meaningful EE point.

(iv) If $\mathcal{R}_0 > 1$, System (1) has exactly one biologically meaningful EE point.

Proof. The nonzero roots of Eq. (20) are given by:

$$\xi^* = \frac{-s_1 \pm \sqrt{s_1^2 - 4s_2s_0}}{2s_2}.$$

Since $\xi^* > 0$ is required for a root to be biologically meaningful, the signs of the roots are

subsequently analyzed based on the value of $\mathcal{R}_0$.

Case 1. If $\mathcal{R}_0 < 1$, then $s_0 < 0$. For $s_1 > 0$, the roots of Eq. (20) have a positive sum and product. Thus, depending on discriminant $D = s_1^2 - 4s_2s_0$, there are two distinct positive roots if $D > 0$, one positive double root if $D = 0$, or no real roots if $D < 0$. The positive real roots indicate the possibility of a backward bifurcation. Conversely, if $s_1 \leq 0$, the roots have a nonpositive sum and a positive product. Hence, no positive real roots exist.

Case 2. If $\mathcal{R}_0 = 1$, then $s_0 = 0$ and Eq. (20) becomes $\xi^*(s_2\xi^* + s_1) = 0$. One root is $\xi^* = 0$, while the nonzero root is given by:

$$\xi^* = -\frac{s_1}{s_2}.$$

Since $s_2 < 0$, the nonzero root is positive if $s_1 > 0$. Thus, one biologically meaningful EE point exists only when $s_1 > 0$. No biologically meaningful EE point exists if $s_1 \leq 0$.

Case 3. If $\mathcal{R}_0 > 1$, then $s_0 > 0$. For $s_1 > 0$, Eq. (20) becomes $s_2\xi^{*2} + s_1\xi^* + s_0 = 0$, whereas for $s_1 < 0$, it becomes $-s_2\xi^{*2} - s_1\xi^* + s_0 = 0$. In both cases, the polynomial has exactly one positive real root. Moreover, since

$$\xi_1^*\xi_2^* = \frac{s_0}{s_2} < 0,$$

the two roots have opposite signs. Hence, there is exactly one biologically meaningful EE point. □

4.6. Bifurcation analysis

The existence of EE points in the first case of Theorem 2 suggests possible backward bifurcation for $\mathcal{R}_0 < 1$. To investigate this at $\mathcal{R}_0 = 1$, we apply the *Center Manifold Theorem* of Castillo-Chavez and Song [43]. The bifurcation direction is determined by coefficients a and b, derived from the system's state-variable and bifurcation-parameter derivatives.

Theorem 3. *The EE point X^* exists and is locally asymptotically stable for $\mathcal{R}_0 > 1$ sufficiently close to 1. Furthermore, System (1) exhibits a forward bifurcation at $\mathcal{R}_0 = 1$.*

Proof. Let $\mathbf{x}$ be the state vector defined in Eq. (2). The parameter e is selected as the bifurcation parameter. Setting $\mathcal{R}_0 = 1$ yields the critical value $e = e^*$, given by:

$$e^* = \frac{c\mu(\eta + \mu + \omega)b_1b_2b_3b_4b_5(\mu_B - \pi_B)}{\beta\pi\left[\alpha_N b_3b_4b_5(\mu p + \eta) + \tau\alpha_M\phi b_1b_2(\sigma_S\gamma_S + \delta + \mu + \varepsilon_S d)(\mu(1-p) + \omega)\right]}, \tag{21}$$

where $b_1, ..., b_5$ are defined in Eq. (11). The Jacobian matrix of System (1) is evaluated at the DFE with $e = e^*$. The corresponding right eigenvector $\mathbf{w}$ associated with the zero eigenvalue is then determined as follows:

$$\mathbf{w} = \begin{bmatrix} w_1 & w_2 & w_3 & w_4 & w_5 & w_6 & w_7 & w_8 & w_9 & w_{10} & w_{11} \end{bmatrix}^T, \tag{22}$$

where

$$w_1 = -\frac{e^*\pi\left(\eta\mu\phi(1-p)+\eta\mu p+\eta\omega\phi+\mu^2 p+\eta^2+\eta\mu\right)w_{11}}{c\mu^2(\eta+\mu+\omega)^2},$$

$$w_5 = -\frac{e^*\pi\left(\mu^2\phi(1-p)+\mu\omega(p+\phi(1-p)+\phi)+\omega^2\phi+\eta\omega\right)w_{11}}{c\mu^2(\eta+\mu+\omega)^2}.$$

$$w_2 = \frac{g_1}{b_1}, \qquad w_3 = \frac{g_1\alpha_N}{b_1 b_2}, \qquad w_4 = \frac{g_1\alpha_N\gamma_N}{b_1 b_2\mu},$$

$$w_6 = \frac{g_2}{b_3}, \qquad w_7 = \frac{g_2\tau\alpha_M}{b_3 b_4}, \qquad w_8 = \frac{g_2\sigma_M\gamma_M\tau\alpha_M}{b_3 b_4\mu},$$

$$w_9 = \frac{g_2\delta\tau\alpha_M}{b_3 b_4 b_5}, \qquad w_{10} = \frac{g_2\sigma_S\gamma_S\delta\tau\alpha_M}{b_3 b_4 b_5\mu}. \qquad w_{11} > 0,$$

and

$$g_1 = \frac{e^*\pi(\mu p+\eta)w_{11}}{c\mu(\eta+\mu+\omega)}, \qquad g_2 = \frac{e^*\pi(\mu(1-p)+\omega)\phi w_{11}}{c\mu(\eta+\mu+\omega)}.$$

Next, the corresponding left eigenvector $\mathbf{v}$ associated with the zero eigenvalue is given by:

$$\mathbf{v}^T = \begin{bmatrix} v_1 & v_2 & v_3 & v_4 & v_5 & v_6 & v_7 & v_8 & v_9 & v_{10} & v_{11} \end{bmatrix}, \tag{23}$$

where

$$v_2 = \frac{\alpha_N\beta v_{11}}{b_1 b_2}, \qquad v_3 = \frac{\beta v_{11}}{b_2}, \qquad v_6 = \frac{\tau\alpha_M\beta(b_5+\delta)v_{11}}{b_3 b_4 b_5},$$

$$v_7 = \frac{\beta(b_5+\delta)v_{11}}{b_4 b_5}, \qquad v_9 = \frac{\beta v_{11}}{b_5}, \qquad v_1 = v_4 = v_5 = v_8 = v_{10} = 0,$$

$$v_{11} = v_{11} > 0.$$

To impose the normalization condition in the *Center Manifold Theorem*, the inner product $\mathbf{v}^T\mathbf{w}$ is evaluated, yielding a nonnegative term. Accordingly, the normalization constants v_{11} and w_{11} are chosen such that $\mathbf{v}^T\mathbf{w} = 1$. The bifurcation coefficients a and b, calculated from the second-order partial derivatives of $\mathbf{f}(\mathbf{x})$ evaluated at X^0 and $e = e^*$, are given by:

$$a = \sum_{\substack{i,j=1\\k=1}}^{n} v_k w_i w_j \frac{\partial^2 f_k}{\partial x_i \partial x_j}\left(X^0, e^*\right), \qquad b = \sum_{i,k=1}^{n} v_k w_i \frac{\partial^2 f_k}{\partial x_i \partial e}\left(X^0, e^*\right). \tag{24}$$

Using the nonzero components of $\mathbf{v}$ and $\mathbf{w}$ and the corresponding second-order partial derivatives, the coefficient a in Eq. (24) simplifies to:

$$a = -\frac{2e^*\pi w_{11}^2}{c^2\mu}\left[v_2\left(\frac{e^*\left(\eta\mu\phi(1-p)+\eta\mu p+\eta\omega\phi+\mu^2 p+\eta^2+\eta\mu\right)}{\mu(\eta+\mu+\omega)^2}+\frac{\mu p+\eta}{\eta+\mu+\omega}\right)\right.$$
$$\left.+\, v_6\phi\left(\frac{e^*\left(\mu^2\phi(1-p)+\mu\omega\left(p+\phi(1-p)+\phi\right)+\omega^2\phi+\eta\omega\right)}{\mu(\eta+\mu+\omega)^2}+\frac{\mu(1-p)+\omega}{\eta+\mu+\omega}\right)\right]. \tag{25}$$

Since all parameters are positive and $0 \le p \le 1$, we have $w_{11} > 0$, $v_2 > 0$, $v_6 > 0$, $e^* > 0$, implying positivity of all bracketed terms. Hence, the negative factor preceding the expression implies that $a < 0$. Next, using the same approach, the coefficient b in Eq. (24) simplifies to:

$$b = \frac{\pi w_{11}}{c\mu(\eta+\mu+\omega)}\left[v_2(\mu p+\eta)+v_6\phi(\mu(1-p)+\omega)\right]. \tag{26}$$

Since all parameters are positive and $0 \leq p \leq 1$, we obtain $w_{11} > 0$, $v_2 > 0$, $v_6 > 0$, ensuring that all terms inside the brackets are positive. Hence, $b > 0$.
Since $a < 0$ and $b > 0$, the model exhibits a forward bifurcation at $e = e^*$, where $\mathcal{R}_0 = 1$. Consequently, a positive, locally asymptotically stable EE exists for $\mathcal{R}_0 > 1$ sufficiently close to 1, whereas the DFE is locally asymptotically stable for $\mathcal{R}_0 < 1$. Thus, $\mathcal{R}_0 = 1$ is the bifurcation threshold. The bifurcation diagram is shown in Fig. 2. □

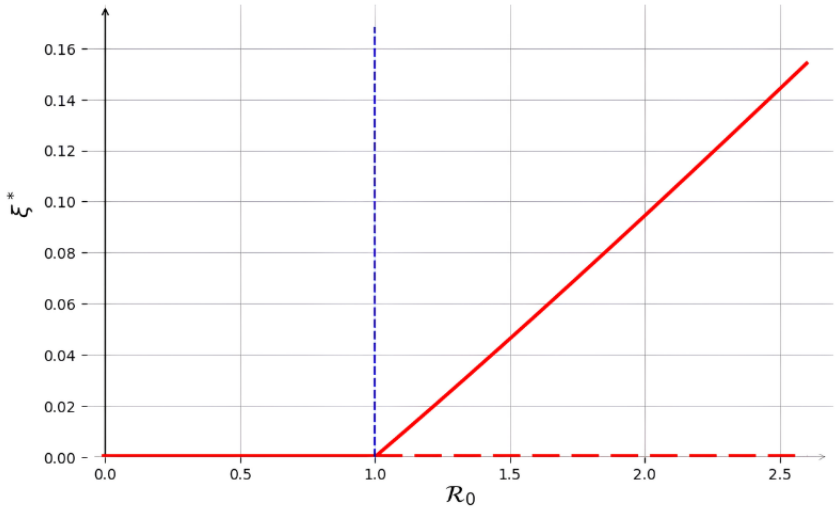


Fig. 2: Bifurcation diagram of system (1)

In the context of the model of this study, the existence of an EE point when $\mathcal{R}_0 > 1$ indicates that persistent TB transmission can maintain the presence of individuals with active TB, including those with moderate stunting, thereby allowing progression toward severe stunting. Therefore, the bifurcation analysis not only identifies the mathematical threshold for TB persistence but also highlights the importance of maintaining transmission dynamics below this threshold to limit TB persistence and its associated consequences for stunting severity among children.

5. Numerical Simulations

Numerical simulations of System (1) were performed over $0 \leq t \leq 40$ years with initial conditions $S_N(0) = S_M(0) = 1200$, $E_N(0) = E_M(0) = 1000$, $I_N(0) = I_M(0) = I_S(0) = 500$, $R_N(0) = R_M(0) = R_S(0) = 300$, and $B(0) = 1000$. Using the parameter values in Table 1, Eq. (7) yields the DFE point X^0, with $S_N^0 = 3726.04$ and $S_M^0 = 3047.21$. From Eq. (12), we obtain $\mathcal{R}_0 = 1.552 > 1$, with contributing proportions of $\mathcal{R}_{0N} \approx 41.17\%$, and $\mathcal{R}_{0M} \approx 58.83\%$. Thus, moderate stunting contributes more to $\mathcal{R}_0$. Since $\mathcal{R}_0 > 1$, TB has the potential to persist under the considered parameter values.

Substituting the parameter values into Eq. (18) yields the EE point X^*, given by $S_N^* = 3045.09$, $E_N^* = 298.78$, $I_N^* = 115.40$, $R_N^* = 131.13$, $S_M^* = 1858.50$, $E_M^* = 271.41$, $I_M^* = 56.12$, $R_M^* = 51.01$, $I_S^* = 66.94$, $R_S^* = 45.64$, and $B^* = 197.08$. The population dynamics in Fig. 3 show that although convergence is not achieved within the simulation period, the trajectories tend toward their respective EE values. The conditions $\mathcal{R}_0 > 1$, $\xi^* > 0$, and $B^* > 0$ support the existence of a biologically meaningful EE, whose local asymptotic stability near $\mathcal{R}_0 = 1$ is established by the bifurcation analysis.

Figure 3(a) shows that $S_N^* > S_M^*$, indicating a larger susceptible population among children with normal nutritional status. This occurs despite the higher rate of nutritional deterioration than improvement ($\omega > \eta$), possibly because of the higher proportion of children entering the model with normal nutritional status, represented by p, compared with those entering with

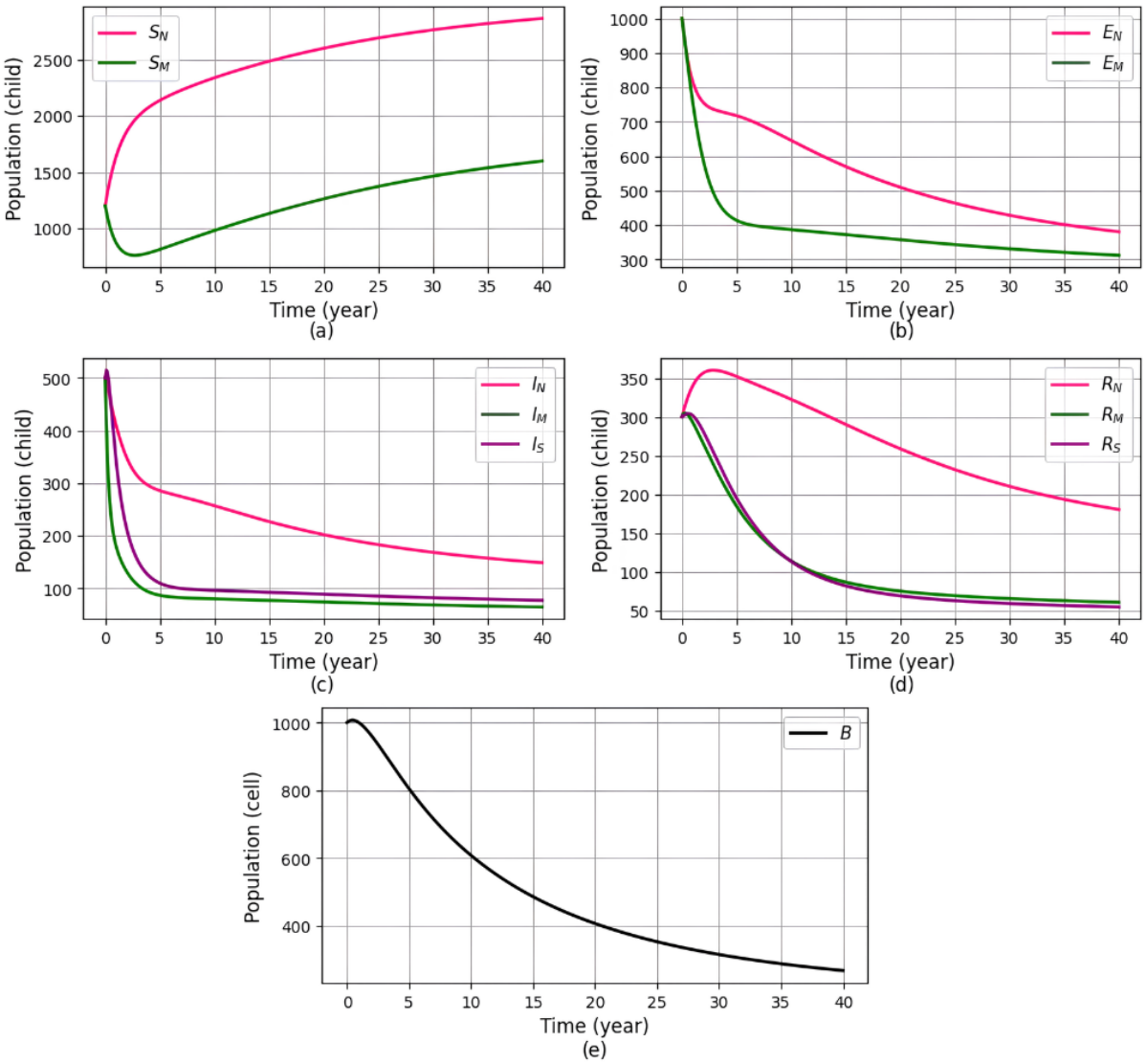


Fig. 3: Dynamical simulations of system (1) based on the parameter values in Table 1 for (a) susceptible (S_N and S_M), (b) latent TB (E_N and E_M), (c) active TB (I_N, I_M, and I_S), (d) recovered (R_N, R_M, and R_S), and (e) viable Mtb in environmental reservoir (B) compartments

moderate stunting, represented by $1 - p$. Similarly, Figure 3(b) shows that $E_N^* > E_M^*$, although the difference is smaller than that between the susceptible populations. This may reflect the increased TB transmission risk among children with moderate stunting, represented by ϕ.

Figure 3(c) shows that $I_N^* > I_S^* > I_M^*$, indicating that children with normal nutritional status have the largest active TB population, consistent with $E_N^* > E_M^*$. Despite the increased TB activation rate associated with τ among children with moderate stunting, their active TB population remains smaller than that of children with normal nutritional status. Meanwhile, $I_S^* > 0$ reflects the progression from moderate to severe stunting at rate δ, while $I_S^* > I_M^*$ suggests a substantial contribution from this transition, consistent with the relatively high value of δ used in the simulation. Figure 3(d) shows that $R_N^* > R_M^* > R_S^*$, with the largest recovered TB population among children with normal nutritional status, consistent with their higher active TB population. The condition $R_M^* > R_S^*$ may be associated with the assumed relationship $\sigma_S < \sigma_M < 1$, which implies lower effective recovery rates with increasing stunting severity.

Children leave all compartments at the rate $\mu = \mu_d + \mu_a = 0.2033$, accounting for natural mortality and aging out. In addition, TB-induced mortality occurs at the baseline rate d and is modified by the multipliers $\varepsilon_M < \varepsilon_S$. This difference may contribute to the higher recovered

population among children with moderate stunting than severe stunting ($R_M^* > R_S^*$), although recovery dynamics are also influenced by the corresponding recovery rates and population inflows. Figure 3(e) shows the persistence of viable Mtb in the environmental reservoir, consistent with $B^* > 0$, together with $\mathcal{R}_0 > 1$. Moreover, $\mu_B - \pi_B = 0.121 > 0$ satisfies the assumption $\mu_B > \pi_B$, indicating that bacterial degradation exceeds bacterial growth.

6. Sensitivity Analysis and Effects of Varying Some Parameters

Sensitivity analysis was conducted using the LHS-PRCC method. LHS divides the range of each parameter into intervals with equal probability and randomly selects one sample from each interval to ensure efficient coverage of the parameter space. The resulting parameter samples and model output are then ranked and regressed against the remaining input parameters. The residuals from these regressions are used to calculate the Pearson correlation coefficient, yielding the PRCC values. PRCC values range from -1 to 1, where a larger absolute value indicates a stronger relationship, while the sign indicates the direction of the relationship between the parameter and the model output [44].

In this study, sensitivity analysis focused on 13 parameters associated with TB transmission, nutritional status progression, and TB progression and recovery, with $\mathcal{R}_0$ as the model output. The analysis was performed using Python, with 10,000 samples generated through LHS based on uniform distributions and a fixed random seed of 8500. Each parameter range was divided into 10,000 equally probable intervals, from which one sample was randomly selected. The parameters were varied within 80%–120% of their reference values listed in Table 1 to assess model sensitivity around these values rather than represent empirical ranges from the literature. The approximate 95% confidence intervals (CIs) of the PRCC values were calculated using the Fisher-z transformation, with the standard error determined by the sample size and number of control variables. The resulting confidence limits were then transformed back to the PRCC scale.

Based on the 10,000 parameter combinations generated through LHS, the resulting $\mathcal{R}_0$ values ranged from 0.6747 to 3.5350, with a mean of 1.5879 and a standard deviation of 0.3949. Among these samples, 387 (3.87%) yielded $\mathcal{R}_0 < 1$, while 9,613 (96.13%) yielded $\mathcal{R}_0 > 1$, indicating that most sampled parameter combinations favor TB transmission and potential disease invasion. These percentages represent the proportions of sampled parameter combinations rather than probabilities of TB occurrence in the actual population. Furthermore, the 95% empirical uncertainty interval, defined by the 2.5th and 97.5th percentiles, ranges from 0.9508 to 2.4995, reflecting the variability in model outputs due to variations in input parameters rather than uncertainty in observational estimates. Since this interval includes the threshold $\mathcal{R}_0 = 1$, it indicates that the sampled parameter variations may lead to different epidemiological outcomes.

The parameter ranges, confidence intervals, and resulting PRCC coefficients are presented in Table 2, based on the reference parameter values in Table 1. For clearer visualization of the PRCC coefficients and their directions, the results are also presented in the bar chart in Fig. 4.

The LHS-PRCC analysis indicates that the parameters with the greatest influence on $\mathcal{R}_0$ are $\mu_B - \pi_B$, β, c, e, and ϕ, as reflected by their large absolute PRCC values. Meanwhile, the parameters α_N, τ, α_M, and ω exhibit relatively weak positive relationships with $\mathcal{R}_0$. In addition, the parameters γ_N, η, γ_M, and δ show relatively weak negative relationships with $\mathcal{R}_0$.

The parameter $\mu_B - \pi_B$, representing the net clearance rate of viable Mtb from the environmental reservoir, has the strongest negative PRCC (-0.9199), indicating that an increase in this parameter is associated with a decrease in $\mathcal{R}_0$, and vice versa. Conversely, β, which represents the contribution of active TB cases to the environmental Mtb reservoir, exhibits a strong positive PRCC (0.9198), indicating that greater bacterial contributions are associated with higher $\mathcal{R}_0$. The parameters c and e also show strong associations with $\mathcal{R}_0$, with PRCC values of -0.9190 and 0.9188, respectively. These are consistent with the force of infection, $\xi = \frac{eB}{c+B}$, whereby an increase in e raises ξ and consequently $\mathcal{R}_0$, whereas an increase in c reduces both. Similarly, ϕ, representing the increased risk of TB infection among children with moderate stunting, has a

Table 2: Parameter ranges and PRCC results with 95% confidence intervals

Parameter	Parameter Range	PRCC	95% CI Lower	95% CI Upper
$\mu_B - \pi_B$	0.0968–0.1452	-0.9199	-0.9229	-0.9169
β	0.08–0.12	0.9198	0.9168	0.9228
c	2000–3000	-0.9190	-0.9220	-0.9159
e	0.56–0.84	0.9188	0.9157	0.9218
ϕ	1.888–2.832	0.8033	0.7963	0.8102
α_N	0.2544–0.3816	0.3457	0.3283	0.3629
τ	1.5680–2.3520	0.3176	0.2999	0.3351
α_M	0.2544–0.3816	0.3019	0.2840	0.3196
ω	0.16–0.24	0.2604	0.2420	0.2786
γ_N	0.1848–0.2772	-0.2529	-0.2712	-0.2345
η	0.08–0.12	-0.1068	-0.1261	-0.0874
γ_M	0.1848–0.2772	-0.0924	-0.1118	-0.0729
δ	1.4124–2.1154	-0.0567	-0.0762	-0.0371

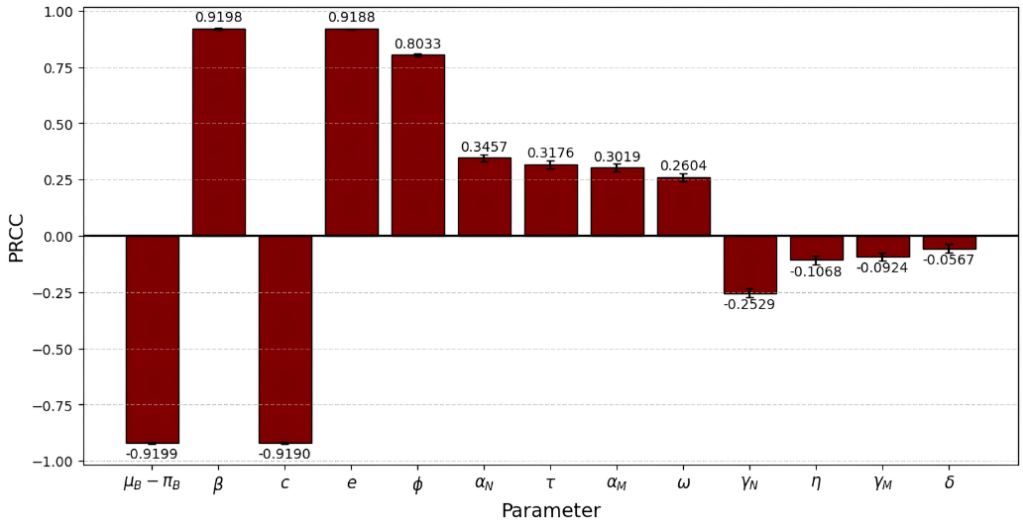


Fig. 4: Partial rank correlation coefficients (PRCC) of model parameters

positive PRCC (0.8033), indicating that higher values are associated with an increase in $\mathcal{R}_0$.

Furthermore, simulations were conducted to examine the effects of variations in four parameters, namely $\mu_B - \pi_B$, e, c, and γ. The first three were selected based on their high absolute PRCC values and the lack of established values. The parameter γ was also included because it represents the recovery rate that can be improved through TB treatment interventions. For simplicity, equal recovery rates were assumed across nutritional-status groups as γ. Each parameter was varied at five levels (60%, 80%, 100%, 120%, and 140% of its reference value). The effects of these variations were evaluated in the compartments associated with each parameter. The simulation results and corresponding percentage changes are presented in Table 3.

Table 3 shows that variations in e considerably affect active TB populations across all nutritional-status groups, with I_N being the most responsive compartment due to its role in determining the force of infection ξ. Interestingly, decreases in e produce greater reductions in active TB populations than the increases resulting from equivalent rises, indicating an asymmetric response. Although all groups are affected, their responses are relatively similar, except at higher parameter values. The corresponding population dynamics are presented in Fig. 5.

Similar to the results for parameter e, variations in c also have a considerable and asymmetric effect on the active TB populations across all nutritional-status groups. The I_N compartment remains the most responsive, with a considerably greater response compared to the other nutritional-status groups. The resulting population dynamics are presented in Fig. 6.

Table 3: Simulation results for variations in e, c, γ, and $\mu_B - \pi_B$

Variation in e across the compartments I_N, I_M, and I_S						
e	I_N	I_N Change	I_M	I_M Change	I_S	I_S Change
0.42	63.3	−57.47%	33.2	−48.64%	40.17	−48.09%
0.56	105.31	−29.24%	50.55	−21.80%	60.73	−21.52%
0.7	148.82	0.00%	64.64	0.00%	77.38	0.00%
0.84	190.71	+28.15%	74.94	+15.93%	89.55	+15.73%
0.98	229.72	+54.36%	82.08	+26.98%	97.99	+26.63%
Variation in c across the compartments I_N, I_M, and I_S						
c	I_N	I_N Change	I_M	I_M Change	I_S	I_S Change
1500	252.27	+69.51%	85.41	+32.13%	101.92	+31.71%
2000	193.09	+29.75%	74.52	+15.28%	90.23	+16.61%
2500	148.82	0.00%	64.64	0.00%	77.38	0.00%
3000	115.82	−22.17%	54.24	−16.09%	65.1	−15.87%
3500	91.22	−38.70%	45.07	−30.28%	54.27	−29.87%
Variation in γ across the compartments R_N, R_M, and R_S						
γ	R_N	R_N Change	R_M	R_M Change	R_S	R_S Change
0.1386	133.16	−26.15%	39.45	−34.90%	36.8	−32.43%
0.1848	159.6	−11.48%	50.48	−16.70%	46.21	−15.15%
0.231	180.3	0.00%	60.6	0.00%	54.46	0.00%
0.2772	196.5	+8.99%	69.88	+15.31%	61.68	+13.26%
0.3234	209.13	+15.99%	78.39	+29.36%	67.97	+24.81%
Variation in $\mu_B - \pi_B$ across the compartment B						
$\mu_B - \pi_B$	B	B Change				
0.0726	664.07	+146.94%				
0.0968	418.44	+55.60%				
0.121	268.92	0.00%				
0.1452	173.66	−35.42%				
0.1694	111.43	−58.56%				

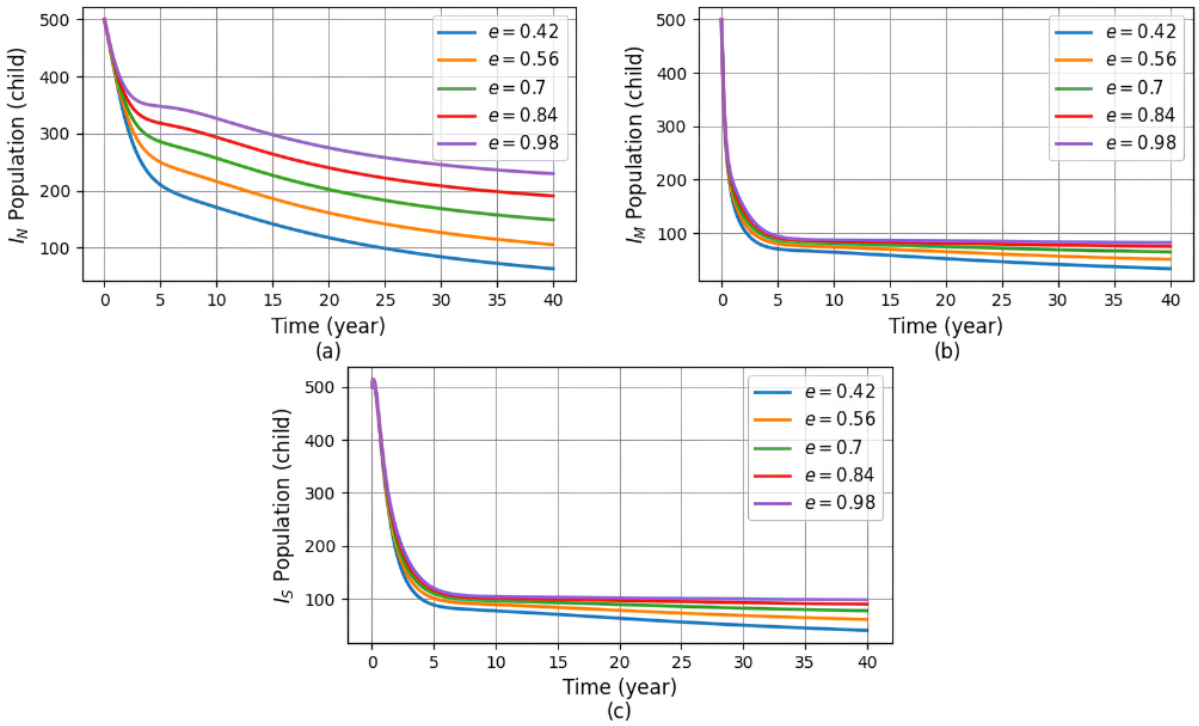


Fig. 5: Dynamic patterns of parameter e variation on compartment (a) I_N, (b) I_M, and (c) I_S

Table 3 shows that γ has a relatively modest effect on $\mathcal{R}_0$, as indicated by its low absolute

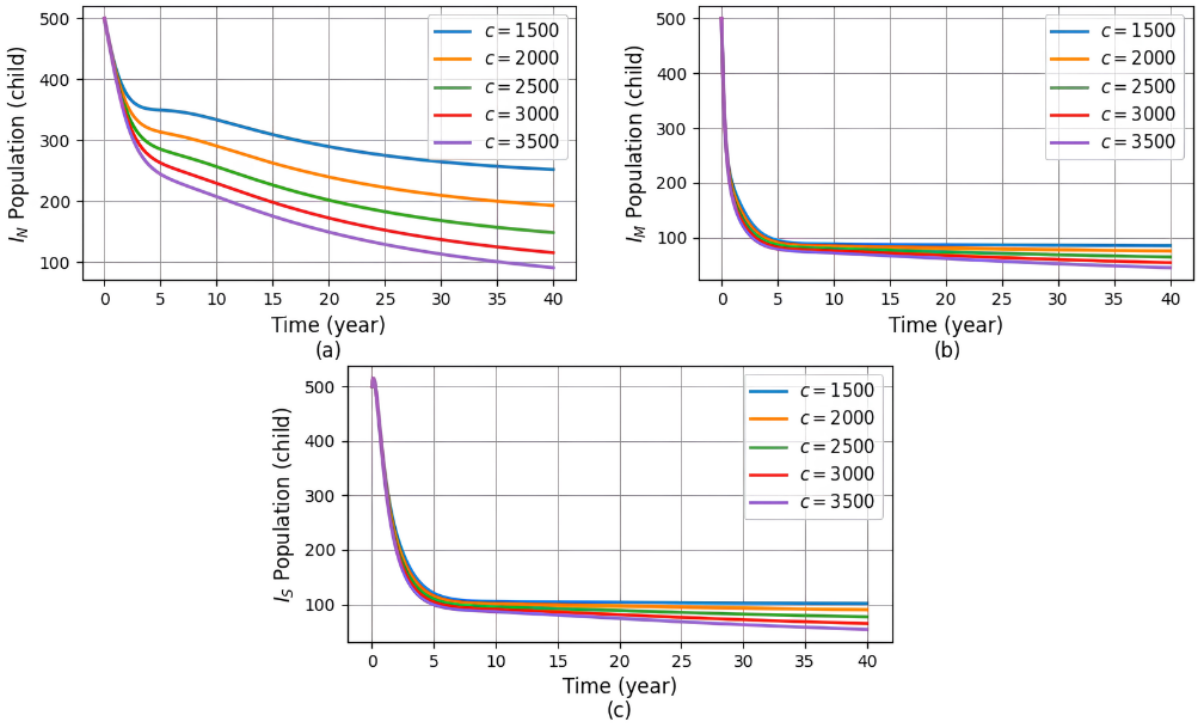


Fig. 6: Dynamic patterns of parameter c variation on compartment (a) I_N, (b) I_M, and (c) I_S

PRCC value. Its negative PRCC reflects the inverse relationship between the recovery rate and $\mathcal{R}_0$. The simulations further show that increasing γ raises the recovered populations across all nutritional-status groups, with R_M exhibiting the greatest relative response, followed by R_S and R_N. This indicates that recovered populations among children with stunting are more responsive to changes in the recovery rate than those among children with normal nutritional status. These differences arise from the combined effects of recovery flows and the overall dynamics of each nutritional-status group. The corresponding population dynamics are presented in Fig. 7.

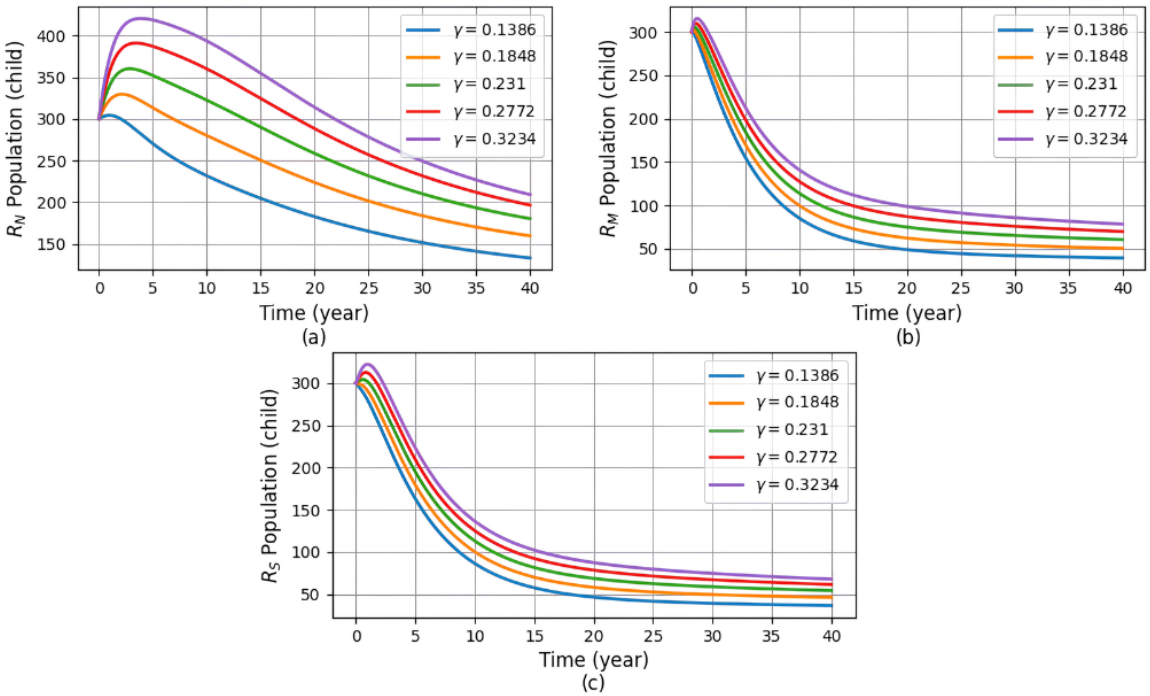


Fig. 7: Dynamic patterns of parameter γ variation on compartment (a) R_N, (b) R_M, and (c) R_S

Finally, Table 3 highlights the effect of variations in the net clearance rate of viable Mtb from the environmental reservoir, represented by $\mu_B - \pi_B$, on the dynamics of compartment B. The results show that decreasing $\mu_B - \pi_B$ increases the amount of Mtb in the environmental reservoir, and vice versa. Interestingly, a decrease in this parameter produces a greater increase in the bacterial population than the reduction resulting from an equivalent increase in the parameter. This indicates an asymmetric response of the environmental Mtb reservoir to variations in the net clearance rate. The corresponding dynamics are presented in Fig. 8.

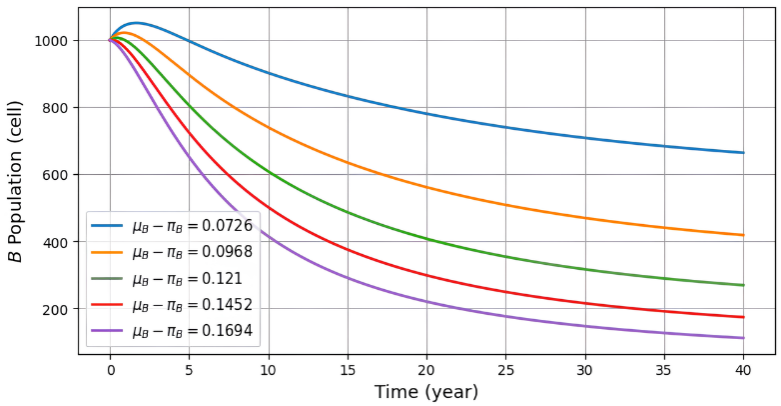


Fig. 8: Dynamic patterns of parameter $\mu_B - \pi_B$ variation on compartment B

In general, the simulation results indicate that parameter variations, even within relatively small ranges, can substantially affect population dynamics. This highlights the importance of accurate parameter estimation in representing TB epidemiological dynamics among children across different nutritional-status groups. However, the limited availability of empirical data for some parameters in this study necessitated the use of estimates and assumptions derived from the literature. This constitutes one of the limitations of the study and should be considered when interpreting the simulation results. Therefore, future research is expected to incorporate more specific empirical data to obtain more accurate parameter estimates, allowing the model to represent TB epidemiological dynamics more realistically.

Based on the sensitivity analysis and numerical simulations, the parameters e, c, and γ have important implications for TB control and reducing $\mathcal{R}_0$. A reduction in e can be achieved by limiting contact with individuals with active TB, implementing appropriate isolation practices, using masks in high-risk settings, and promoting respiratory hygiene. Although c, which determines the response of the transmission rate to the amount of Mtb in the environmental reservoir, cannot be directly modified through interventions, measures such as improving ventilation, reducing crowding in enclosed spaces, and using respiratory protection can help limit exposure to airborne Mtb. Meanwhile, increasing γ through early TB detection, appropriate treatment, and adherence to prescribed treatment regimens can promote recovery from active TB. Overall, these findings emphasize the importance of reducing TB exposure and transmission while improving treatment outcomes among children across different nutritional-status groups.

7. Discussion

Poor nutritional status can increase the risk of TB, while TB infection can further worsen nutritional status, creating a bidirectional relationship between the two conditions. Previous mathematical models have investigated the relationship between TB and nutritional status [25, 27, 28], incorporated environmental reservoirs as sources of TB transmission [29], or considered stunting in TB models, although not specifically in children populations [30]. However, no previous studies have simultaneously considered the progression of stunting from moderate to severe and the presence of viable Mtb in environmental reservoirs, particularly among children, despite the epidemiological relevance of these factors [19, 21, 24].

The mathematical analysis confirms the biological feasibility of the developed model through the nonnegativity of its compartments and the positive invariance of the feasible region. The model has two equilibrium points, with the DFE derived explicitly and the EE implicitly. The basic reproduction number, $\mathcal{R}_0$, is derived using the NGM method. Based on Jacobian eigenvalues, the DFE has been proven to be locally asymptotically stable when $\mathcal{R}_0 < 1$. The existence of the EE is examined by determining the roots of an equation in ξ and establishing conditions for biologically feasible solutions. The *Center Manifold Theorem* reveals a forward bifurcation at $\mathcal{R}_0 = 1$, with a locally asymptotically stable EE emerging for $\mathcal{R}_0 > 1$ sufficiently close to 1, indicating the potential for sustained TB transmission.

Sensitivity analysis was conducted using the LHS-PRCC method to assess the effects of 13 parameters on $\mathcal{R}_0$. A total of 10,000 samples were generated from uniform distributions within 80%–120% of reference values using random seed 8500. PRCC values and 95% confidence intervals were calculated to evaluate the strength and direction of parameter relationships with $\mathcal{R}_0$. The resulting values ranged from 0.6747 to 3.5350, with a mean of 1.5879 and a standard deviation of 0.3949. Most samples (96.13%) yielded $\mathcal{R}_0 > 1$, while 3.87% yielded $\mathcal{R}_0 < 1$. The 95% empirical uncertainty interval was 0.9508–2.4995, encompassing the threshold $\mathcal{R}_0 = 1$. Thus, despite varying outcomes, most sampled parameter combinations favored TB transmission.

The LHS-PRCC analysis identifies $\mu_B - \pi_B$, β, c, e, and ϕ as the most influential parameters on $\mathcal{R}_0$. Variations in $\mu_B - \pi_B$, c, e, and γ were further investigated through numerical simulations. The results show that even relatively small parameter variations can substantially affect population dynamics. In particular, decreasing e and increasing c and γ reduce active TB populations, consistent with their effects on $\mathcal{R}_0$ and the force of infection ξ. These findings suggest that TB control efforts should focus on reducing exposure to infectious sources, improving ventilation, reducing crowding in enclosed spaces, and implementing appropriate respiratory protection and hygiene practices. Meanwhile, increasing the recovery rate can be supported through early TB detection and diagnosis, appropriate treatment, and adherence to treatment completion.

Nevertheless, this study has limitations related to its simplifying assumptions and parameter estimation. The model assumes restricted nutritional transitions, specific progression pathways to severe stunting, unchanged nutritional status after TB recovery, and permanent immunity. Additionally, some parameter values rely on literature-based estimates due to limited empirical data, while the LHS-PRCC ranges may not fully capture parameter variability. These limitations should be considered when interpreting the model results and their epidemiological implications.

8. Conclusion

This study develops a mathematical epidemiological model of childhood TB that integrates TB transmission dynamics with changes in nutritional status, including the progression of stunting severity, and the presence of viable Mtb in environtmental reservoir. The developed model is mathematically proven to have nonnegative compartments and a positively invariant feasible region, confirming its biological feasibility.

The analysis established the existence of the DFE and EE, with the DFE being locally asymptotically stable when $\mathcal{R}_0 < 1$. Furthermore, the bifurcation analysis revealed a forward bifurcation at $\mathcal{R}_0 = 1$, with the EE emerging and being locally asymptotically stable for $\mathcal{R}_0 > 1$ sufficiently close to 1. Numerical simulations showed that the solutions approach the EE, consistent with the analytical findings. The LHS-PRCC analysis identified $\mu_B - \pi_B$, β, c, e, and ϕ as the most influential parameters on $\mathcal{R}_0$. Further simulations demonstrated that decreasing e and increasing c and γ reduce active TB populations.

Future studies should incorporate more specific empirical data on childhood TB and nutritional status to improve parameter estimation and model validity. Furthermore, relaxing the simplifying assumptions regarding nutritional transitions, disease recovery, and immunity may provide a more representative of the interaction between TB in children and nutritional status.

CRediT Authorship Contribution Statement

Ranti Rivani Aisyah: Conceptualization, Investigation, Methodology, Data Curation, Formal Analysis, Software, Validation, Visualization, Writing–Original Draft, Writing–Review & Editing, Project Administration. **Nursanti Anggriani:** Supervision, Writing–Review & Editing. **Anita Triska:** Supervision, Writing–Review & Editing.

Declaration of Generative AI and AI-assisted technologies

During the preparation of this manuscript, the authors used ChatGPT (GPT-5.6 Luna) for translation from Indonesian into English and for language editing to improve the clarity and grammatical correctness of the manuscript. The authors reviewed and edited all AI-assisted text and take full responsibility for the final content of the manuscript.

Declaration of Competing Interest

The authors declare no competing interests.

Ethics Approval and Consent to Participate

Ethics approval was not required for this study.

Funding and Acknowledgments

This research received no external funding. The authors would like to express their gratitude to Universitas Padjadjaran for providing the academic environment and resources for this research.

Data and Code Availability

The data supporting the findings of this study are derived from previously published sources cited in the manuscript. The code used for the mathematical modeling, numerical simulations, and sensitivity analysis is available from the corresponding author upon reasonable request.

References

[1] M. Sarkar and J Sarkar. “Transmission of Mycobacterium Tuberculosis”. In: *Journal of The Association of Physicians of India* 73.9 (2025), pp. 91–96. DOI: 10.59556/japi.73.1113.

[2] World Health Organization. *Global Tuberculosis Report 2025*. Geneva: World Health Organization, 2025. https://www.who.int/publications/i/item/9789240116924.

[3] M. Sarkar. “Incipient and Subclinical Tuberculosis: A Narrative Review”. In: *Monaldi Archives for Chest Disease* 96.1 (2026), p. 2982. DOI: 10.4081/monaldi.2025.2982.

[4] H. Esmail, L. Macpherson, A. K. Coussens, et al. “Mind the Gap - Managing Tuberculosis Across the Disease Spectrum”. In: *eBioMedicine* 78.4 (2022), p. 103928. DOI: 10.1016/j.ebiom.2022.103928.

[5] J. Creswell and C. Colvin. “Closing the Gaps in Childhood TB Detection”. In: *IJTLD Open* 2.2 (2025), pp. 83–89. DOI: 10.5588/ijtldopen.24.0494.

[6] B. K. Moore, S. M. Graham, S. Nandakumar, et al. “Pediatric Tuberculosis: A Review of Evidence-Based Best Practices for Clinicians and Health Care Providers”. In: *Pathogens* 13.6 (2024), p. 467. DOI: 10.3390/pathogens13060467.

[7] S. Menon, A. D. Harries, R. A. Dlodlo, et al. “Series 2: Invisible Threats: A Global Scoping Review of Risk Factors for Tuberculosis Infection”. In: *Tropical Medicine and Infectious Disease* 11.4 (2026), p. 87. DOI: 10.3390/tropicalmed11040087.

[8] N. Siddalingaiah, K. Chawla, S. B. Nagaraja, and D. Hazra. "Risk Factors for the Development of Tuberculosis Among the Pediatric Population: A Systematic Review and Meta-Analysis". In: *European Journal of Pediatrics* 182.7 (2023), pp. 3007–3019. DOI: 10.1007/s00431-023-04988-0.

[9] L. Martinez, R. Verma, J. Croda, et al. "Detection, Survival and Infectious Potential of Mycobacterium tuberculosis in the Environment: A Review of the Evidence and Epidemiological Implications". In: *European Respiratory Journal* 53.6 (2019), p. 1802302. DOI: 10.1183/13993003.02302-2018.

[10] D. O. Matuka, T. Duba, Z. Ngcobo, et al. "Occupational Risk of Airborne Mycobacterium tuberculosis Exposure: A Situational Analysis in a Three-Tier Public Healthcare System in South Africa". In: *International Journal of Environmental Research and Public Health* 18.19 (2021), p. 10130. DOI: 10.3390/ijerph181910130.

[11] K. Middelkoop, A. S. Koch, Z. Hoosen, et al. "Environmental Air Sampling for Detection And Quantification of Mycobacterium Tuberculosis in Clinical Setting: Proof of Concept". In: *Infection Control and Hospital Epidemiology* 44 (2023), pp. 774–779. DOI: 10.1017/ice.2022.162.

[12] E. W. Bunyasi, K. Middelkoop, A. Koch, et al. "Molecular Detection of Airborne Mycobacterium tuberculosis in South African High Schools". In: *American Journal of Respiratory and Critical Care Medicine* 205.3 (2022), pp. 350–356. DOI: 10.1164/rccm.202102-0405OC.

[13] United Nations Children's Fund (UNICEF), World Health Organization (WHO), and International Bank for Reconstruction and Development/The World Bank. *Levels and Trends in Child Malnutrition: UNICEF/WHO/World Bank Group Joint Child Malnutrition Estimates: Key Findings of the 2025 Edition*. Geneva: World Health Organization, 2025. https://www.who.int/publications/i/item/9789240112308.

[14] P. K. Sahoo, A. Swain, and B. Mishra. "A Comprehensive Analysis of Stunting Syndrome in Children in Developing Countries: A Comprehensive Review". In: *Research and Reviews in Pediatrics* 25.1 (2024), pp. 12–15. DOI: 10.4103/rrp.rrp_4_24.

[15] World Health Organization. *WHO Child Growth Standards: Length/Height-for-Age, Weight-for-Age, Weight-for-Length, Weight-for-Height and Body Mass Index-for-Age: Methods and Development*. Geneva: World Health Organization, 2006. https://www.who.int/publications/i/item/924154693X.

[16] S. K. Das, A. D. Burma, S. Amudhan, V. Mishra, et al. "Do Children in India Grow Well Into Adolescents? Longitudinal Analysis of Growth Transitions From Young Lives Panel Survey in India". In: *Public Health* 202 (2022), pp. 18–25. DOI: 10.1016/j.puhe.2021.10.010.

[17] M. S. Oduro, S. Iddi, L. Asiedu, et al. "Utilizing a Multi-Stage Transition Model for Analysing Child Stunting in Two Urban Slum Settlements Of Nairobi: a Longitudinal Analysis, 2011-2014". In: *PLOS ONE* 19.2 (2024), e0272684. DOI: 10.1371/journal.pone.0272684.

[18] C. van Zyl and C. van Wyk. "Exploring Factors That Could Potentially Have Affected the First 1000 Days of Absent Learners in South Africa: A Qualitative Study". In: *International Journal of Environmental Research and Public Health* 18.5 (2021), p. 2768. DOI: 10.3390/ijerph18052768.

[19] N. T. Ozer and K. Gundogan. "The Vicious Cycle of Malnutrition and Tuberculosis: A Narrative Review". In: *Journal of Clinical Practice and Research* 46.5 (2024), pp. 444–448. DOI: 10.14744/cpr.2024.60895.

[20] J. V. A. Franco, B. Bongaerts, M. I. Metzendorf, et al. "Undernutrition as a Risk Factor for Tuberculosis Disease". In: *Cochrane Database of Systematic Reviews* 6 (2024), p. CD015890. DOI: 10.1002/14651858.CD015890.pub2.

[21] B. T. Haerana, N. A. Prihartono, P. Riono, et al. "Prevalence of Tuberculosis Infection and Its Relationship to Stunting in Children (Under Five Years) Household Contact with New Tuberculosis Cases". In: *Indian Journal of Tuberculosis* 68.3 (2021), pp. 350–355. DOI: 10.1016/j.ijtb.2020.10.011.

[22] C. Y Wu, C. C. Ku, C. F. McQuaid, et al. "Estimating the Impact of Nutritional Transition and Ending Hunger on Tuberculosis in 12 High-Burden Countries: A Model-Based Scenario Analysis". In: *BMJ Global Health* 10.12 (2025), e018839. DOI: 10.1136/bmjgh-2024-018839.

[23] A. S. Izza, Martini, M. S. Adi, et al. "Nutritional Status and Tuberculosis Among Children Under Five in Indonesia: A Systematic Review and Meta-Analysis". In: *Journal of Communicable Diseases* 57.4 (2025), pp. 93–104. DOI: 10.24321/0019.5138.2026102.

[24] H. M. Nataprawira and C. Cesilia. "Tuberculosis (TB) Status in Under-Five Children with Stunting in Bandung". In: *Global Pediatric Health* 11 (2024), pp. 1–7. DOI: 10.1177/2333794X241304375.

[25] L. O. Sabran, L. Annur, and A. R. Laura. "Dynamic Analysis of the Mathematical Model for Stunting With Nutrition and Education Interventions". In: *BAREKENG: Journal of Mathematics and Its Applications* 19.4 (2025), pp. 2317–2334. DOI: 10.30598/barekengvol19iss4pp2317-2334.

[26] F. Inayaturohmat, N. Anggriani, A. K. Supriatna, et al. "A Systematic Literature Review of Mathematical Models for Coinfections: Tuberculosis, Malaria, and HIV/AIDS". In: *Journal of Multidisciplinary Healthcare* 17 (2024), pp. 1091–1109. DOI: 10.2147/JMDH.S446508.

[27] E. P. Yusdini and I. Sukarsih. "Model Matematika Penyebaran Penyakit Tuberkulosis dengan Faktor Gizi dan Penggunaan Masker Medis". In: *Jurnal Riset Matematika* 5.1 (2025), pp. 81–90. DOI: 10.29313/jrm.v5i1.6762.

[28] R. Yadav and N. Goel. "Mathematical Model for Analysing the Interplay Between Income, Nutrition, and Tuberculosis Dynamics". In: *Computers in Biology and Medicine* 196 (2025), p. 110858. DOI: 10.1016/j.compbiomed.2025.110858.

[29] Y. A. Liana, J. Z. Ndendya, and N. Shaban. "The Nutritional Nexus: Modeling the Impact of Malnutrition on TB Transmission". In: *Scientific African* 27 (2025), e02516. DOI: 10.1016/j.sciaf.2024.e02516.

[30] R. Amelia, N. Anggriani, and W. M. A. W. Ahmad. "An Integrated Optimal Control Model for Simultaneous Tuberculosis Transmission and Stunting Prevention". In: *Mathematics* 14.7 (2026), p. 1140. DOI: 10.3390/math14071140.

[31] C. M. Faye, S. Fonn, and J. Levin. "Factors associated with recovery from stunting among under-five children in two Nairobi informal settlements". In: *PLOS ONE* 14.4 (2019), e0215488. DOI: 10.1371/journal.pone.0215488.

[32] D. R. Sjarif, K. Yuliarti, L. C. Gultom, et al. "Effectiveness of a Tiered Referral System and Early Nutritional Intervention to Prevent and Recover Stunting in Under-Five Indonesian Children". In: *Food Science & Nutrition* 13.10 (2025), e70945. DOI: 10.1002/fsn3.70945.

[33] J. Benjamin-Chung, A. Mertens, J. M. Colford, et al. "Early-Childhood Linear Growth Faltering in Low- and Middle-Income Countries". In: *Nature* 621.7979 (2023), pp. 550–557. DOI: 10.1038/s41586-023-06418-5.

[34] Badan Pusat Statistik. *Hasil Survei Penduduk Antar Sensus (SUPAS 2025)*. Tech. rep. 51/05/Th. XXIX. Jakarta: Badan Pusat Statistik, May 2026.

[35] S. Arregui, M. J. Iglesias, S. Samper, et al. "Data-Driven Model for the Assessment of Mycobacterium Tuberculosis Transmission in Evolving Demographic Structures". In: *Proceedings of the National Academy of Sciences* 115.14 (2018), E3238–E3245. DOI: 10.1073/pnas.1720606115.

[36] G. L. Becker, P. Amuge, R. Ssebunya, et al. "Predictors of Mortality in Ugandan Children with TB, 2016-2021". In: *The International Journal of Tuberculosis and Lung Disease* 27.9 (2023), pp. 668–674. DOI: 10.5588/ijtld.22.0622.

[37] B. J. Vonasek, K. K. Radtke, P. Vaz, et al. "Tuberculosis in Children with Severe Acute Malnutrition". In: *Expert Review of Respiratory Medicine* 16.3 (2022), pp. 273–284. DOI: 10.1080/17476348.2022.2043747.

[38] R. Ragonnet, J. A. Flegg, S. L. Brilleman, et al. "Revisiting the Natural History of Pulmonary Tuberculosis: A Bayesian Estimation of Natural Recovery and Mortality Rates". In: *Clinical Infectious Diseases* 73.1 (2021), e88–e96. DOI: 10.1093/cid/ciaa602.

[39] R. Diel and A. Nienhaus. "Pathways of TB Transmission in Children—A Systematic Review of Molecular Epidemiological Studies". In: *International Journal of Environmental Research and Public Health* 20.3 (2023), p. 1737. DOI: 10.3390/ijerph20031737.

[40] C. T. Codeço. "Endemic and Epidemic Dynamics of Cholera: The Role of the Aquatic Reservoir". In: *BMC Infectious Diseases* 1.1 (2001), p. 1. DOI: 10.1186/1471-2334-1-1.

[41] P. van den Driessche and J. Watmough. "Reproduction Numbers and Sub-threshold Endemic Equilibria for Compartmental Models of Disease Transmission". In: *Mathematical Biosciences* 180.1-2 (2002), pp. 29–48. DOI: 10.1016/S0025-5564(02)00108-6.

[42] J. C. Kamgang and G. Sallet. "Computation of Threshold Conditions for Epidemiological Models and Global Stability of the Disease-Free Equilibrium (DFE)". In: *Mathematical Biosciences* 213.1 (2008), pp. 1–12. DOI: 10.1016/j.mbs.2008.02.005.

[43] C. Castillo-Chavez and B. Song. "Dynamical Models Of Tuberculosis And Their Applications". In: *Mathematical Biosciences and Engineering* 1.2 (2004), pp. 361–404. DOI: 10.3934/mbe.2004.1.361.

[44] S. Marino, I. B. Hogue, C. J. Ray, and D. E. Kirschner. "A Methodology for Performing Global Uncertainty and Sensitivity Analysis in Systems Biology". In: *Journal of Theoretical Biology* 254.1 (2008), pp. 178–196. DOI: 10.1016/j.jtbi.2008.04.011.